Hindawi
Mathematical Problems in Engineering
Volume 2019, Article ID 3483516, 10 pages
https://doi.org/10.1155/2019/3483516

Research Article

Mathematical Expression of Design Hysteretic Energy Spectra Based on Chinese Soil Type

Cuiling Ma,[1,2] **Qiang Gu**,[1,3] **and Guohua Sun**[3]

[1]*College of Civil and Transportation Engineering, Hohai University, Nanjing 210098, China*
[2]*Department of Civil Engineering, Hefei University, Hefei 230601, China*
[3]*School of Civil Engineering, Suzhou University of Science and Technology, Suzhou 215011, China*

Correspondence should be addressed to Cuiling Ma; ling3701@163.com

Received 17 October 2018; Revised 28 January 2019; Accepted 18 February 2019; Published 2 April 2019

Academic Editor: Giovanni Falsone

This paper explores the energy-based seismic design based on source-to-site distance and the site classification found in Chinese national codes. Specifically, 750 ground motion records were selected according to Chinese site classification, and the equivalent velocity spectra of cumulative hysteretic energy (HE) demand were derived using the energy-balance equation with the single degree of freedom (SDOF) system. In addition, the effects of soil type, earthquake magnitude, site group, structural damping ratio, and ductility ratio were investigated on the HE spectra, and mathematical expression of the equivalent velocity spectrum was presented. The analysis of the HE spectra indicated that the HE spectra were significantly affected by the ground acceleration amplitude, soil type, site group, and damping ratio. The ductility ratio also had an impact on the spectral value, but no effect on the spectral shape. The effect of postyielding stiffness ratio (PYSR) on the spectral shape and spectral value could be neglected. The research findings shed new light on the seismic design based on HE spectrum.

1. Introduction

The conventional force-based seismic design method can only take into account the effect of maximum response while cumulative damage resulting from numerous inelastic cycles cannot be precisely accounted for (Fajfar and Vidic [1]). Also, the displacement-based seismic design cannot appropriately consider the component of damage that is related to the cumulative plastic strain energy (López-Almansa et al. [2]). The energy-based seismic design is known for the consideration of structural strength and displacement and the cumulative damage caused by persistent ground motion. This type of design reflects more ground motion features than force- and displacement-based seismic designs. Since Housner [3] introduced a seismic design methodology based on energy concept, this more rational seismic design approach in terms of energy is gaining extensive attention (Akiyama [4, 5]; Uang and Bertero [6]; Goel [7]; Leelataviwat et al. [8]; Choi and Kim [9]; Sahoo and Chao [10]; Kharmale and Ghosh [11]; Habibi et al. [12]; Heidari and Gharehbaghi [13]).

The energy-based seismic design considers that a structure can survive under a severe earthquake if the structural energy supply is greater than the energy demand. The input energy to an ordinary structure subjected to strong ground motions can be resolved into kinetic energy, elastic strain energy, damping energy, and the hysteretic energy (HE). In energy-based seismic design, the HE demand plays an important role as it is related to the cumulative structural damage that resulted from seismic activity. Various forms of energy spectra have been created, thanks to its simplicity, convenience, and close correlation with seismic codes. Mckevitt et al. [14] analyzed the HE of multistory buildings under seismic excitation. They found that a majority of the HE dissipated from the bottom floor of the structure, while the stiffness and strength were distributed uniformly along the structure's height. Akiyama [4]considered that the input energy is a very stable quantity and proposed the energy spectrum in terms of a bilinear relationship. Fajfar and Vidic [1]derived approximately the inelastic spectra for hysteretic and input energy from the elastic spectrum by

using the dimensionless parameters. Bruneau and Wang [15] developed the normalized HE spectra for a simple SDOF system subjected to the simple rectangular pulse and sine-wave ground excitations. Chou and Uang [16] established an attenuation relationship of the absorbed energy from a two-stage nonlinear regression analysis for a given earthquake magnitude, source-to-site distance, site class, and ductility factor. Resulting from the study of a large set of strong motion records, Decanini and Mollaioli [17] obtained inelastic design input energy spectra for the evaluation of energy seismic demand as a function of soil type, ductility, source-to-site distance, and magnitude. Then, the spectra of the hysteretic to input energy ratio were evaluated for different target ductility ratios and soil types. Khashaee P. [18] established a HE spectrum considering the field effects and ground motion features. Through nonlinear dynamic analysis, López-Almansa et al. [2]obtained an equivalent velocity ratio spectrum of the HE and the input energy from the record of strong earthquakes in Turkey, with the consideration of the impacts of soil type and earthquake magnitude. Dindar et al. [19] derived the input and plastic energy demand spectra directly from the energy-balance equation, considering different soil types, elastic perfectly plastic constitutive model, 5% viscous damping ratio, different ductility levels, and varying seismic intensities. In view of the effects of multidirectional earthquake excitations, Wang et al. [20, 21] constructed the mean normalized input energy spectra and HE spectra and created a normalized HE spectrum of constant ductility ratios to estimate the story HE demand, where the normalized HE is defined as the ratio of the HE to the square of the peak ground acceleration (PGA). Sun et al. [22] defined the ratio of the equivalent velocity of HE to the peak ground velocity (PGV) as a dimensionless parameter β_{Eh} and applied it to the indirect calculation of the HE. Dogru et al. [23] evaluated the energy parameters in terms of total energy input and hysteretic energy for special steel concentrically braced frames (CBFs) with different height, assessed the variation of HE along the frame height by nonlinear dynamic time history analysis, and eventually derived the seismic energy demand spectrum and HE distributions of the CBFs.

However, the existing HE spectra are not applicable in China, because all of them are based on non-Chinese site classifications. In Chinese codes, the building sites are divided into five classes, each of which is further split into three groups according to the source-to-site distance and the predominant period of ground motion (T_{g}).

To solve the problem, 750 ground motion records were selected according to Chinese site classification, and the equivalent velocity spectra of cumulative HE demand were derived by the energy-balance equation of single degree of freedom (SDOF) system. Besides, the authors investigated the effects of soil type, earthquake magnitude, site group, structural damping ratio, and ductility ratio on the HE spectra and presented the mathematical expression of equivalent velocity spectrum.

2. Energy-Balance Equation

As stated by Bruneau and Wang [24], it is reasonable to calculate the seismic input energy by the relative energy equation. Under the unidirectional horizontal ground motion, the relative motion equation of an elastic-plastic SDOF system can be expressed as follows:

$$m\ddot{x} + c\dot{x} + f_s = m\ddot{x}_g \tag{1}$$

where m is the mass; c is the viscous damping coefficient; f_{s} is the restoring force; x, $\dot{x}$, and $\ddot{x}$ are the relative displacement, velocity, and acceleration of the mass with respect to ground, respectively; $\ddot{x}_g$ is the ground acceleration.

The energy equation can be derived from (1) through integration over the duration of the earthquake:

$$\int_0^{\mathrm{t}} m\ddot{x}\dot{x}\,dt + \int_0^t c\dot{x}\dot{x}\,dt + \int_0^t f_s\dot{x}\,dt = -\int_0^t m\ddot{x}_g\dot{x}\,dt \tag{2}$$

where t is time.

Equation (2) can be rewritten as

$$E_{K\mathrm{r}} + E_D + E_E + E_H = E_{I\mathrm{r}} \tag{3}$$

where $\mathrm{E_{kr}}$ is the kinetic energy; E_D is the energy dissipated from the viscous damping; $\mathrm{E_E}$ is the elastic strain energy stored in the SDOF system; $\mathrm{E_H}$ is the HE dissipated from inelastic behaviors; $\mathrm{E_{Ir}}$ is the total input energy caused by the earthquake.

In far-field earthquakes, the main cause of structural failure is the cumulative damage from the cyclic effect and gradual accumulation of seismic energy in the structure. Thus, the cumulative HE is a reasonable indicator of far-field seismic damage. Then, $\mathrm{E_H}$ can be expressed as an equivalent velocity V_{EH} (Chou and Uang [25]):

$$V_{EH} = \sqrt{\frac{2E_H}{m}} \tag{4}$$

where m is the mass.

3. Ground Motion Records

A total of 750 ground motion records were extracted from PEER Ground Motion Database according to geological conditions of abundant stations determined by Geng [26], Guo [27], and Zhao [28] with reference to *Code for Seismic Design of Building* [29] of China. Tables 1 and 2 list the number and percentage of records in each soil type, respectively.

In Chinese codes, according to the equivalent shear wave velocity of the soil layer and the thickness of the site cover, the building sites can be divided into soil types I, II, III, and IV, among which soil type I is divided into $\mathrm{I_0}$ and $\mathrm{I_1}$ subclasses. It should be mentioned that Lv [30], by analyzing a number of geological prospecting data of US station sites, concluded

Table 1: Statistics of ground motion records based on moment magnitude according to soil type of Chinese code.

Soil type		Moment magnitude					
		4<M≤5	5<M≤6	6<M≤7	7<M≤8	Total	Proportion
Soil type *I*	I_0	0	1	45	9	55	7.3%
	I_1	0	3	55	7	65	8.7%
Soil type *II*		0	64	387	78	529	70.5%
Soil type *III*		2	0	73	8	83	11.1%
Soil type *IV*		0	4	8	6	18	2.4%
Total		2	72	568	108	750	
Percentage		0.3%	9.6%	75.7%	14.4%		

Table 2: Statistics of ground motion records based on epicenter distance according to soil type of Chinese code.

Soil type		Epicenter distance (km)						
		30<R≤50	50<R≤80	80<R≤120	120<R≤200	200<R	Total	Proportion
Soil type *I*	I_0	14	16	6	12	7	55	7.3%
	I_1	12	22	8	12	11	65	8.7%
Soil *II*		120	128	89	106	86	529	70.5%
Soil *III*		8	21	12	20	22	83	11.1%
Soil *IV*		2	6	2	6	2	18	2.4%
Total		156	193	117	156	128	750	
Percentage		20.8%	25.7%	15.6%	20.8%	17.1%		

that China's soil type I corresponds to site classes A and B and a part of site class C of USA, China's soil type II is between site classes C and D of USA, China's soil type III is between site classes D and E of USA, and China's soil type IV is identical with US site class E.

In the national code mentioned above, the characteristic period T_g (the predominant period of ground motion) is adopted to measure the impacts of seismic environment on the acceleration response spectrum. Here, T_g is calculated by the formula $T_g = 2\pi(v_E/a_E)$. The values of a_E and v_E were calculated as 1/4 of the platform values corresponding to the absolute acceleration response spectrum and pseudovelocity response spectrum, respectively.

The damping ratios of both spectra were assumed as 0.05.

It can be seen from Figure 1 that T_g is closely related to the spectral characteristic index V/A, which is the ratio of PGV and PGA of the ground motion. T_g increases with the increase of V/A. In Figure 2, T_g is generally positively correlated with earthquake magnitude and epicenter distance. As shown in Figures 1 and 2, T_g reflects the overall influence of site conditions, earthquake magnitude, and epicentral distance on ground motion.

Following the *Seismic Ground Motion Parameter Zonation Map of China* [31], the ground motion records of each soil type (I_0, I_1, II, III, and IV) in Table 3 were further split into three site groups according to T_g.

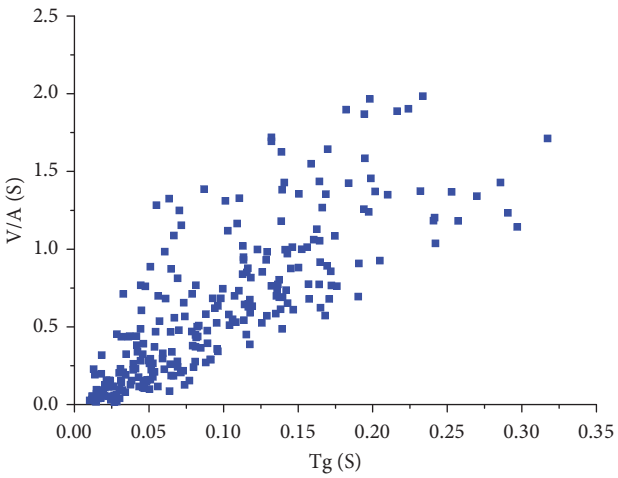

Figure 1: Tg and V/A relationship of soil type II.

4. Parameters Considered in the Study

There are two determinants of the cumulative HE spectra, namely, the features of the estimated seismic oscillation at a given site, such as soil type, acceleration amplitude, and site group, and the dynamic behaviour and nonlinear features of the structure, including structural damping ratio, ductility ratio, and PSYR.

5. Influence of the Parameters in the Hysteretic Energy Spectra

This section probes into the impacts of soil type, acceleration amplitude, site group, and structural damping ratio, ductility ratio, and PSYR on the HE demand of the SDOF system per unit mass, which is represented by equivalent velocity V_{EH}. The target SDOF system obeys the force-displacement

Table 3: Classified standard of ground motion based on Tg(sec).

Site group	Soil type				
	I_0	I_1	II	III	IV
Group 1	≤0.20	≤0.25	≤0.40	≤0.50	≤0.70
Group 2	0.20-0.30	0.25-0.35	0.40-0.45	0.50-0.65	0.70-0.90
Group 3	≥0.30	≥0.35	≥0.45	≥0.65	≥0.90

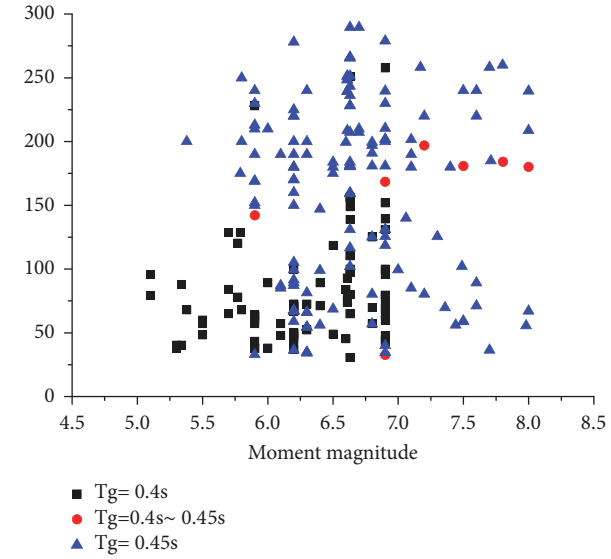

Figure 2: Epicenter distance and earthquake magnitude relationship of soil type II with different T_g.

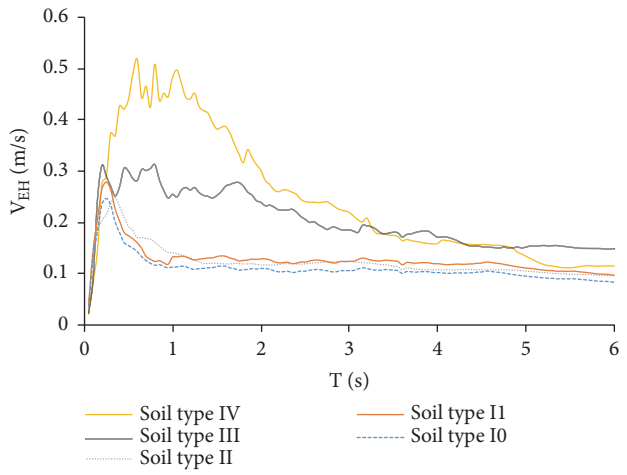

Figure 3: Effect of soil type: μ=2, p=0.0, and ζ=0.05.

relationship given by the bilinear elastic-plastic model. The PYSR was set to 0.05 and 0.00; the damping ratio was configured as ζ=0.01~0.20; the ductility ratio was initialized as μ=1~10.

5.1. Soil Type. The mean V_{EH} under the ground motions of site group 1 of soil types I_0, I_1, II, III, and IV (Table 3) were computed at the PGA of 0.2g, the ductility ratio of 2, the damping ratio of 0.05, and the PSYR of 0.00.

As shown in Figure 3, the soil type exhibits a significant impact on the HE. The mean equivalent velocity spectra consisted of the rising, stable, and declining segments, which correspond to the short, medium, and long periods, respectively. The equivalent velocity spectra of soil types I and II are relatively stable in the long term, but that of soil type IV plunges with the increase of the period. The equivalent velocity spectrum of soil type III appears between those of soil types I and II and soil type IV. The peak equivalent velocity and peak period increase continuously from soil types I to IV.

5.2. Acceleration Amplitude. Amplitude is one of major parameters to measure seismic intensity, such as PGA, PGV, and PGD (peak ground displacement), and the PGA is widely used. As shown in Figure 4, the V_{EH} spectra of two ground motions (RSN2362 and RSN3450) were established for the elastic-plastic SDOF system at the peak PGAs of 0.2g, 0.4g, and 0.52g, ζ=0.05, μ=2, and p =0.05.

It can be seen that the shape of the V_{EH} spectra remains basically the same throughout the period, despite the variation in PGA amplitude, while the V_{EH} values are positively proportional to the amplitude.

5.3. Damping Ratio. The mean V_{EH} spectra of site groups 1, 2, and 3 in soil type II at different damping ratios are presented in Figure 5 (PGA=0.2g, μ=2, p =0.0, and ζ=0.01, 0.02, 0.035, 0.05, 0.10, and 0.20). As can be seen from the figure, the spectra exhibit a negligible shift towards the right with the increase in the damping ratio. Additionally, the peak V_{EH} of each site group drops gradually, indicating the peak clipping effect of the damping ratio. As mentioned in Section 1, Akiyama [4] concluded the input energy, a very stable amount, depends exclusively on the total mass and the fundamental natural period, scarcely dependent on other structural properties such as damping, yield shear strength, and hysteretic loop shapes. Previous studies showed that both the kinetic energy and elastic strain energy, defined in (3), are so small as to be almost negligible, and the input energy is mainly composed of damping energy and hysteretic energy. The damping energy varies with variation of the damping ratio, and the hysteretic energy (in terms of an equivalent velocity V_{EH} in this paper) also changes.

The damping ratio effects have similar impacts on the V_{EH} spectra, under the ground motions of different site groups at different soil types. This means the effects of damping ratio on peak V_{EH} can be expressed by the same correction factor.

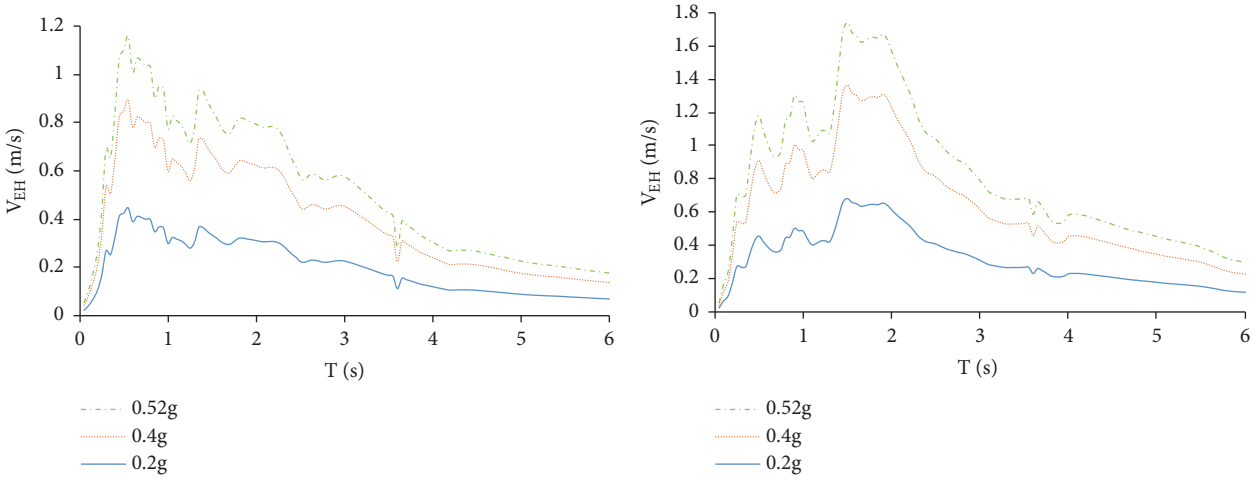

(a) μ=2, p=0.05, and ζ=0.05, ground motion RSN2362

(b) μ=2, p=0.05, and ζ=0.05, ground motion RSN3450

Figure 4: Effect of acceleration amplitude.

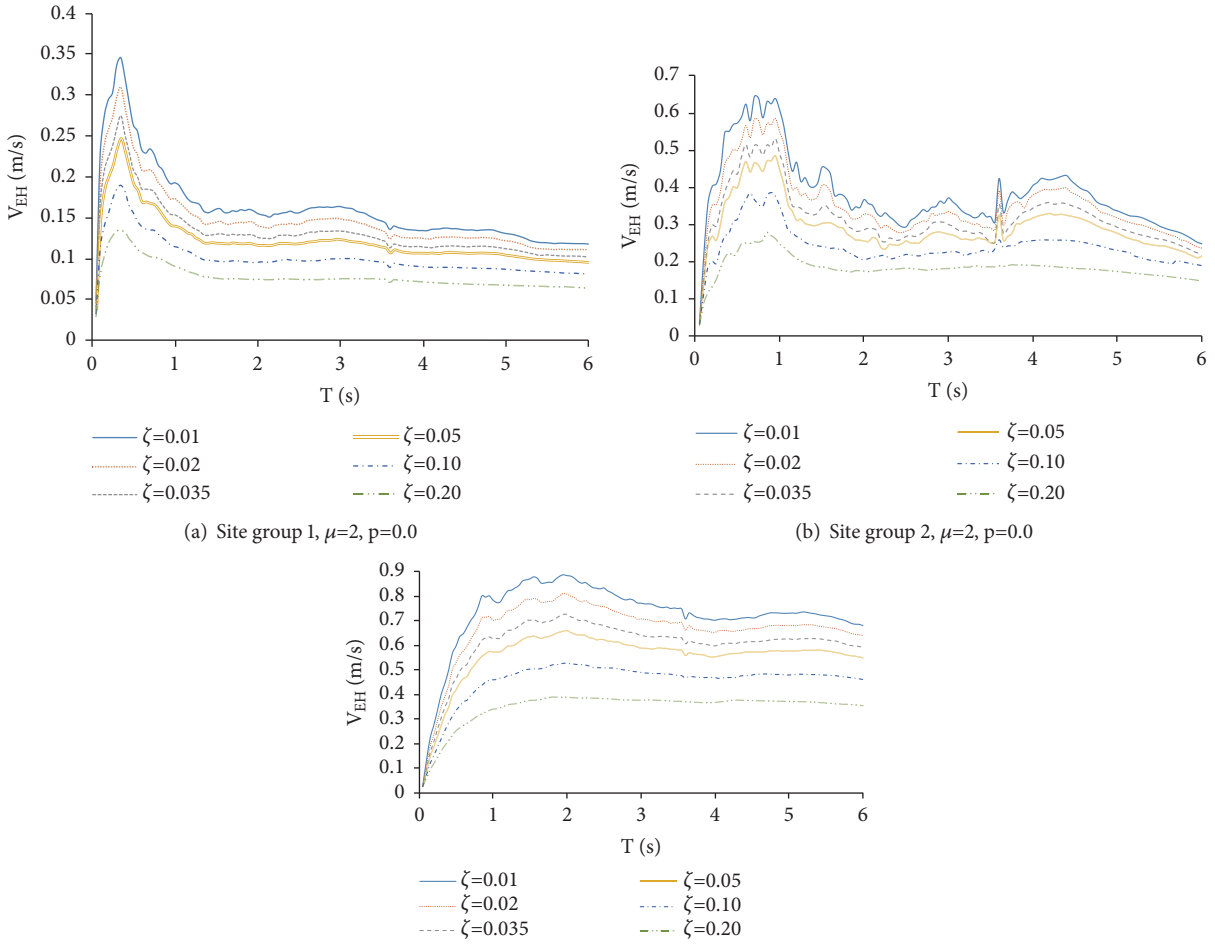

(a) Site group 1, μ=2, p=0.0

(b) Site group 2, μ=2, p=0.0

(c) Site group 3, μ=2, p=0.0

Figure 5: Effects of structural damping ratio.

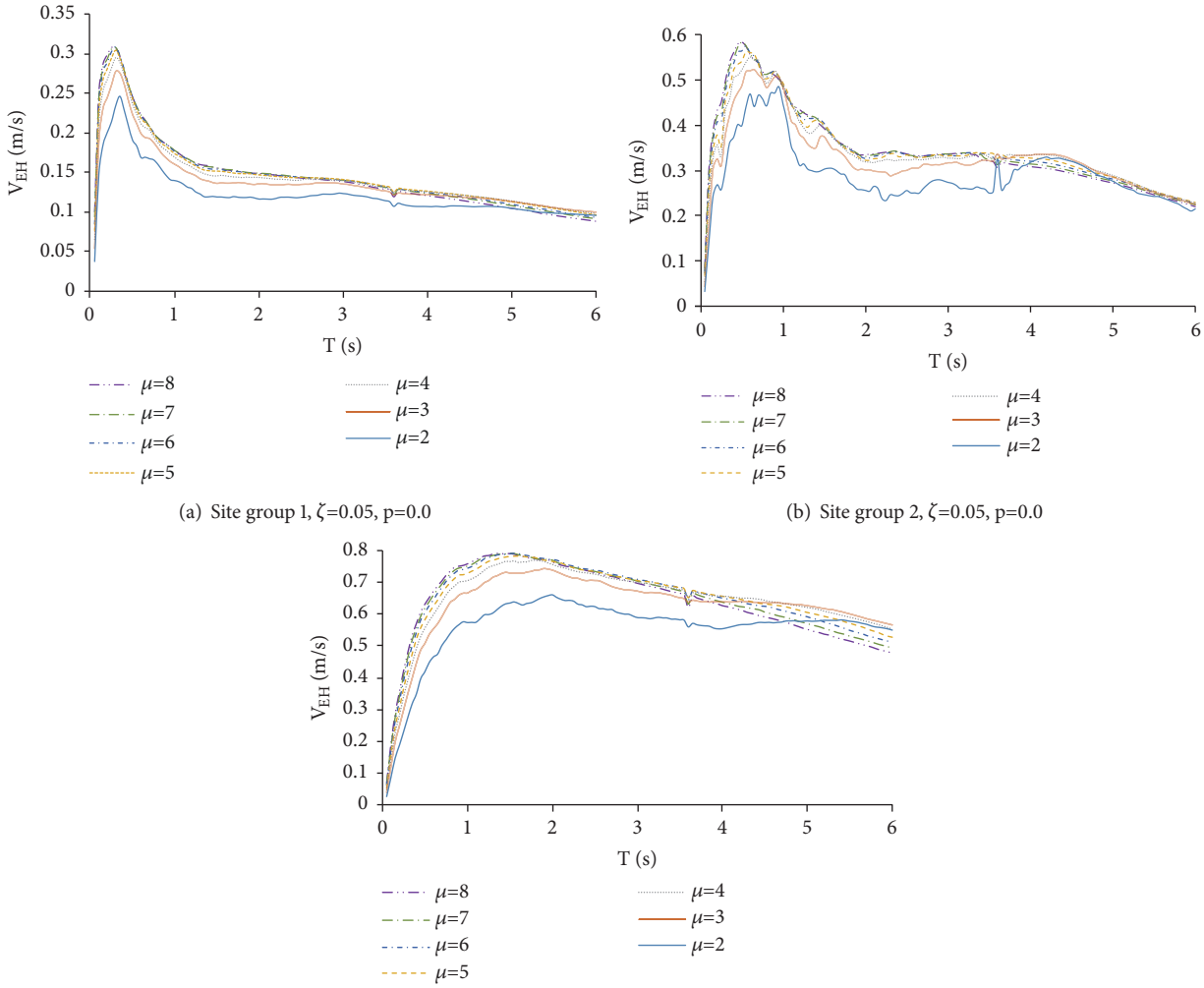

(a) Site group 1, ζ=0.05, p=0.0

(b) Site group 2, ζ=0.05, p=0.0

(c) Site group 3, ζ=0.05, p=0.0

Figure 6: Effect of structural ductility.

5.4. Ductility Ratio. The mean V_{EH} spectra of site groups 1, 2, and 3 in soil type II at different ductility ratios are presented in Figure 6 (PGA=0.2g, ζ=0.05, p=0.0, and μ=2, 3, 4, 5, 6, 7, and 8). As shown in Figure 6, the V_{EH} spectral values are sensitive to small variations in ductility ratio at a given damping ratio. When the ductility ratio grows from 2 to 4, the V_{EH} value at constant period increases continuously but tends to stability when the ductility ratio reaches and surpasses 5. Hence, it can be deduced that the ductility ratio has a limited effect of spectral shape.

5.5. Site Group. The mean V_{EH} spectra of site groups 1, 2, and 3 in soil type II are displayed in Figure 7 at PGA=0.2g, μ=2, p=0.05, and ζ=0.05. Figure 7 shows that the site group has an obvious effect on the HE for the same soil type. The V_{EH} spectral values increase linearly in the short period when the site group changes from 1 to 3.

5.6. Postyielding Stiffness Ratio. The mean V_{EH} spectra of 50 random ground motions of soil type II at different PYSRs were recorded in Figure 8 (PGA=0.2g, μ=2, ζ=0.05, and p=0.0, 0.02, 0.05, 0.10, 0.20, and 0.50). It is clear that the shapes and values of the V_{EH} spectra remain relatively stable with the increase of the PYSR, indicating that the V_{EH} spectra are insensitive to the PYSR. Hence, the effect of the PYSR on the V_{EH} spectra is ignored in the subsequent analysis.

6. Proposed Hysteretic Energy Spectra in Terms of Equivalent Velocity

As mentioned above, the mean equivalent velocity spectra of cumulative HE consist of the rising, stable, and declining segments, and the spectral values are influenced by the acceleration amplitude, soil type, site group, damping ratio, and ductility ratio. In light of these, 15 groups of ground motions were classified by soil type and site group and taken as the inputs. Then, the mean response of each group of ground motions was computed for the statistical analysis on the impacts from the damping ratio, ductility ratio, and the

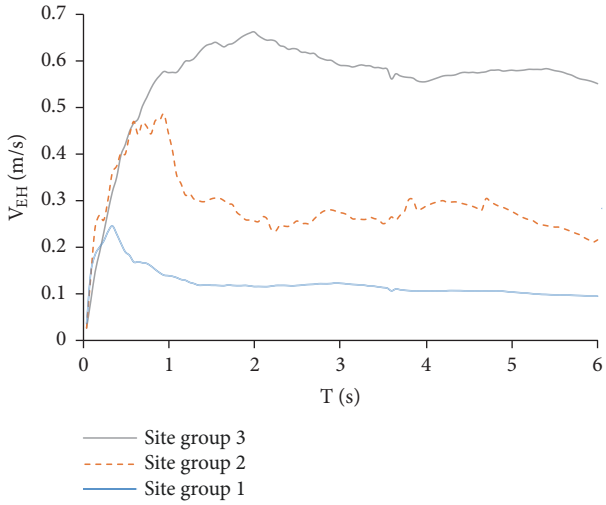

Figure 7: Effect of site group (μ=2, p=0.05, and ζ=0.05).

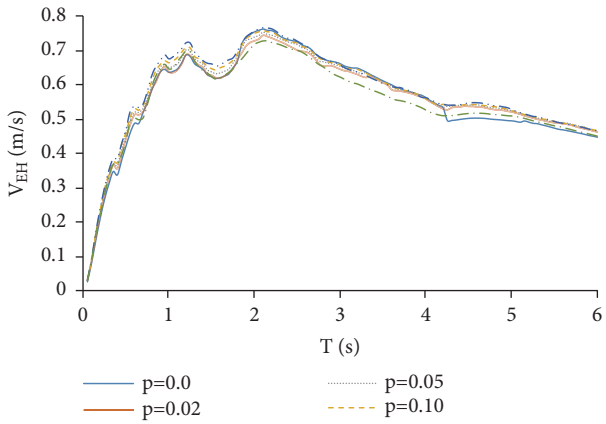

Figure 8: Effect of structural post stiffness ratio (μ=2, ζ=0.05).

PSYR. The fitted smooth spectral curves are presented in Figure 9.

The corresponding mathematical expressions are as follows:

$$V_{EH} = \left(\frac{T}{T_1}\right)\eta_1\eta_2 R_{EH,\mu} V_{EH,max} \quad 0 \le T < T_1$$

$$V_{EH} = \eta_1\eta_2 R_{EH,\mu} V_{EH,max} \quad T_1 \le T \le T_2 \tag{5}$$

$$V_{EH} = \left(\frac{T_2}{T}\right)^{\gamma}\eta_1\eta_2 R_{EH,\mu} V_{EH,max} \quad T_2 < T \le 6$$

where T_1 is the separation period between the rising segment and stable segment; T_2 is the separation period between the stable segment and declining segment; η_1 is the correction factor of acceleration amplitude (see (6)); η_2 is the correction factor of damping ratio (see (7)); $R_{EH,\mu}$ is the correction factor of ductility ratio (see (8)); γ is the attenuation index of the declining segment (see (9)); $V_{EH,\max}$ is the peak equivalent velocity of cumulative HE at the acceleration amplitude of 0.2g, damping ratio of 0.05, the PSYR of 0.0, and the ductility ratio of 2. Note that T_1 and T_2 are related to soil type, site group, and ductility ratio, but not the damping ratio.

(1) Correction Factor of Acceleration Amplitude (η_1). The previous analysis shows that the peak value of equivalent velocity spectra is positively correlated with the acceleration amplitude of ground motion. Thus, the correction factor can be defined as

$$\eta_1 = \frac{\ddot{x}_g}{\ddot{x}_{0.2g}} \tag{6}$$

where $\ddot{x}_g$ is the acceleration amplitude of ground motion and $\ddot{x}_{0.2g}$ is the acceleration amplitude corresponding to $V_{EH,\max}$.

(2) Correction Factor of Damping Ratio (η_2). The reference damping ratio of the elastic-plastic system was set to 0.05. By considering the peak clipping effect of damping ratio on the equivalent velocity spectra of cumulative HE, the correction factor can be defined as follows:

$$\eta_2 = \frac{V_{EH,max,\zeta}}{V_{EH,max,\zeta=0.05}} \tag{7}$$

By comparing the peak values of equivalent velocity spectra at different damping ratios, it was found that the peak value decreased continuously with the increase of the damping ratio. However, the decrease had nothing to do with soil type or site group. Hence, η_2 can be fitted by an inverse proportional function:

$$\eta_2 = 1 + \frac{0.05 - \zeta}{0.1 + 1.5\zeta} \tag{8}$$

where ζ is the structural damping ratio.

(3) Correction Factor of Ductility Ratio ($R_{EH,\mu}$). The values and shapes of the equivalent velocity spectra are sensitive to μ when the latter is smaller than 5. Hence, the correction factor ($R_{EH,\mu}$) can be defined as follows:

$$R_{EH,\mu} = 1 + \frac{\mu - 2}{2.5 + 2\mu} \tag{9}$$

where μ is the ductility ratio.

(4) Attenuation Index of the Declining Segment (γ). As shown in Figure 5, the declining segment tended to be stable with the increase of damping ratio. The attenuation index, $\gamma = \gamma_1 + f(\zeta)$, was introduced to consider the shape variation of the equivalent velocity spectra. Note that the value of $f(\zeta)$ varies with site groups. For safety and simplicity, $f(\zeta)$ was set to a small value under the constant ζ. γ can be expressed as follows:

$$\gamma = \gamma_1 + \frac{0.05 - \zeta}{0.4 + 6\zeta} \tag{10}$$

where the values of γ_1 are listed in Table 4, which are related to soil type and site group and ζ is the damping ratio.

(5) Periods (T_1, T_2) of Characteristic Points. The periods, T_1 and T_2, correspond to the starting and end points of the

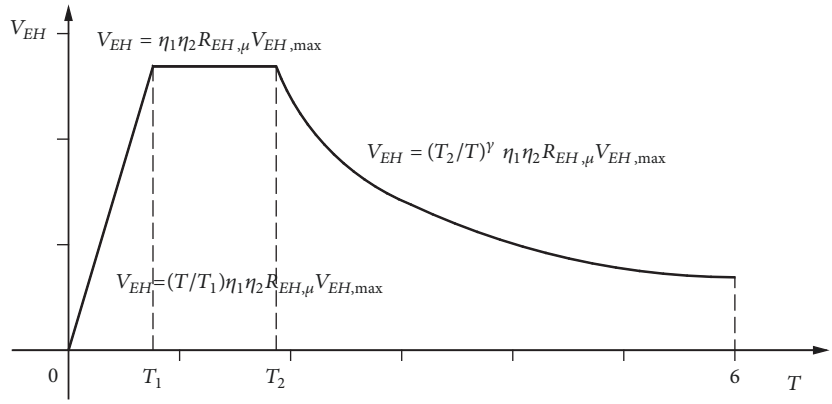

Figure 9: Three-segment model of equivalent velocity spectra of accumulated hysteretic energy.

Table 4: Equivalent velocity spectra parameters when acceleration amplitude is 0.2g.

Soil type	Site group	$V_{EH,\max}$ (m/s)	T_1 (S)	T_2 (S)	γ_1
I_0	Group 1	0.14	0.09	0.38	0.28
	Group 2	0.30	0.31	0.71	0.46
	Group 3	0.52	0.73	2.28	0.31
I_1	Group 1	0.18	0.12	0.42	0.32
	Group 2	0.38	0.37	0.77	0.50
	Group 3	0.58	0.77	2.34	0.35
II	Group 1	0.24	0.20	0.45	0.3
	Group 2	0.45	0.40	1.10	0.4
	Group 3	0.65	0.95	2.2	0.2
III	Group 1	0.30	0.20	1.0	0.35
	Group 2	0.40	0.40	2.0	0.75
	Group 3	0.75	1.20	4.70	0.82
IV	Group 1	0.48	0.40	1.25	0.90
	Group 2	0.55	0.60	1.20	1.00
	Group 3	1.20	0.85	4.85	1.20

horizontal segment, respectively. Their values are related to soil type, site group, and ductility ratio. However, their correlations with damping ratio are so small as to be negligible. There is a certain linear relationship between $T_1(T_2)$ and μ:T_1(or T_2) = $k\mu + b, (k < 0, b > 0)$. For simplicity, the effect of μ is neglected and the values of T_1 and T_2 are extracted from Table 4.

(6) Peak Equivalent Velocity ($V_{EH,max}$). As shown in Table 4, $V_{EH,\max}$ is the peak equivalent velocity in the stable segment at the acceleration amplitude of 0.2g. Here, the mean equivalent velocities of each site group and soil type were selected and fitted by the genetic algorithm on the MATLAB. Figures 10 and 11, respectively, present the fitted equivalent velocity spectra and the dynamic analysis results at different parameters.

7. Conclusions

Considering the importance of structure energy demand in energy-based seismic design, the equivalent velocity spectrum according to Chinese soil site classification was established and the influencing factors on the shapes and peak values of the spectra were discussed in this paper. Through the analysis, the following conclusions can be derived:

(1)The soil type, site group, acceleration amplitude, and damping ratio all have significant effects on the equivalent velocity spectra. When the soil type changed from I to IV, both the peak equivalent velocity and characteristic period increase continuously. The acceleration amplitude has no impact on the shapes of the energy spectra but influences the spectral value. The damping ratio has a peak clipping effect on the equivalent velocity spectra, and the effect remains the same in different site groups. For the same soil type, the peak equivalent velocity increases significantly as the site group shifted from 1 to 3.

(2)The shapes of equivalent velocity spectra have nothing to do with ductility ratio, while the spectral values are positively correlated with structural ductility when $\mu \leq 4$ and remain stable when$\mu \geq 5$. The PYSR has a negligible effect on the shapes and values of equivalent velocity spectra.

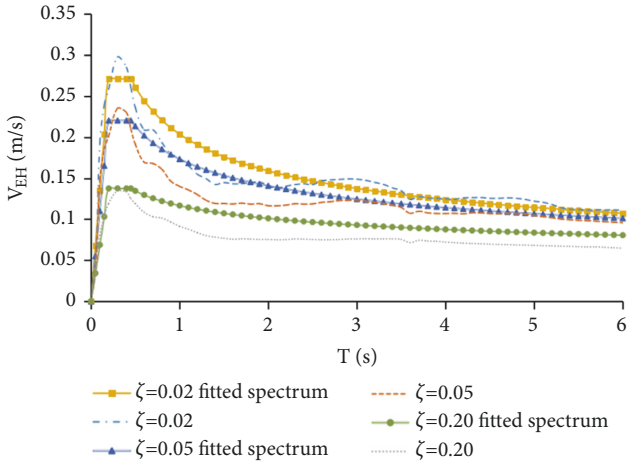

Figure 10: Comparison between fitted equivalent velocity spectra and the dynamic analysis results of group 1 in soil type II under different damping ratios (μ=2 and p=0).

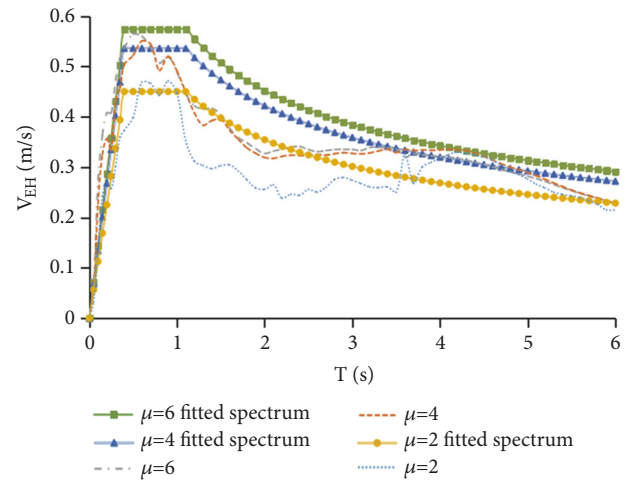

Figure 11: Comparison between fitted equivalent velocity spectra and the dynamic analysis results of group 2 in soil type II under different ductility factors (ζ=0.05 and p=0).

(3)The equivalent velocity spectra consist of a rising segment, a stable segment, and a declining segment. The separation periods T_1 and T_2 are related to soil type, site group, and ductility ratio, but not the damping ratio.

Data Availability

The data used to support the findings of this study are available from the corresponding author upon request.

Conflicts of Interest

The authors declare that there are no conflicts of interest regarding the publication of this paper.

Acknowledgments

This research was funded by the National Natural Science Foundation of China (Grant no. 51278320) and Natural Science Foundation of Hefei University (Grant no. 18ZR14ZDA), which are gratefully acknowledged.

References

[1] P. Fajfar and T. Vidic, "Consistent inelastic design spectra: hysteretic and input energy," *Earthquake Engineering & Structural Dynamics*, vol. 23, no. 5, pp. 523–537, 1994.

[2] F. López-Almansa, A. U. Yazgan, and A. Benavent-Climent, "Design energy input spectra for high seismicity regions based on Turkish registers," *Bulletin of Earthquake Engineering*, vol. 11, no. 4, pp. 885–912, 2013.

[3] G. W. Housner, "Limit design of structures to resist earthquakes," in *Proceedings of the 1st World Conference Earthquake Engineering*, Berkeley, Calif, USA, 1956.

[4] H. Akiyama, *Earthquake-resistant Limit State Design for Buildings*, University of Tokyo Press, Tokyo, Japan, 1985.

[5] H. Akiyama, "Earthquake resistant design based on the energy concept," in *Proceedings of the 9th World Conference on Earthquake Engineering*, Tokyo, Japan, 1988.

[6] C. M. Uang and V. V. Bertero, "Evaluation of seismic energy in structures," *Earthquake Engineering & Structural Dynamics*, vol. 19, no. 1, pp. 77–90, 1990.

[7] R. K. Goel, "Seismic response of asymmetric system: energy-based approach," *Journal of Structural Engineering*, vol. 123, no. 11, pp. 1444–1453, 1997.

[8] S. Leelataviwat, S. C. Goel, and B. Stojadinović, "Energy-based seismic design of structures using yield mechanism and target drift," *Journal of Structural Engineering*, vol. 128, no. 8, pp. 1046–1054, 2002.

[9] H. Choi and J. Kim, "Energy-based seismic design of buckling-restrained braced frames using hysteretic energy spectrum," *Engineering Structures*, vol. 28, no. 2, pp. 304–311, 2006.

[10] D. R. Sahoo and S. Chao, "Performance-based plastic design method for buckling-restrained braced frames," *Engineering Structures*, vol. 32, no. 9, pp. 2950–2958, 2010.

[11] S. B. Kharmale and S. Ghosh, "Performance-based plastic design of steel plate shear wall," *Journal of Constructional Steel Research*, vol. 90, no. 5, pp. 85–97, 2013.

[12] A. Habibi, R. W. Chan, and F. Albermani, "Energy-based design method for seismic retrofitting with passive energy dissipation systems," *Engineering Structures*, vol. 46, pp. 77–86, 2013.

[13] A. Heidari and S. Gharehbaghi, "Seismic performance improvement of special truss moment frames using damage and energy concepts," *Earthquake Engineering & Structural Dynamics*, vol. 44, no. 7, pp. 1055–1073, 2015.

[14] W. E. McKevitt, D. L. Anderson, and S. Cherry, "Hysterretic energy spectra in seismic design," in *Proceedings of the 2nd World Conference on Earthquake Engineering*, pp. 487–494, 1980.

[15] M. Bruneau and N. Wang, "Normalized energy-based methods to predict the seismic ductile response of SDOF structures," *Engineering Structures*, vol. 18, no. 1, pp. 13–28, 1996.

[16] C.-C. Chou and C.-M. Uang, "Establishing absorbed energy spectra - An attenuation approach," *Earthquake Engineering & Structural Dynamics*, vol. 29, no. 10, pp. 1441–1455, 2000.

[17] L. D. Decanini and F. Mollaioli, "An energy-based methodology for the assessment of seismic demand," *Soil Dynamics and Earthquake Engineering*, vol. 21, no. 2, pp. 113–137, 2001.

[18] P. Khashaee, *Energy-Based Seismic Design And Damage Assessment for Structures [Doctor's Thesis]*, School of Engineering, Southern Methodist University, Dallas, Tex, USA, 2004.

[19] A. A. Dindar, C. Yalçın, E. Yüksel, H. Özkaynak, and O. Büyüköztürk, "Development of earthquake energy demand spectra," *Earthquake Spectra*, vol. 31, no. 3, pp. 1667–1689, 2015.

[20] F. Wang, H. Li, and T. Yi, "Energy spectra of constant ductility factors for orthogonal bidirectional earthquake excitations," *Advances in Structural Engineering*, vol. 18, no. 11, pp. 1887–1899, 2015.

[21] F. Wang, H. Li, and N. Zhang, "A method for evaluating earthquake-induced structural damage based on displacement and hysteretic energy," *Advances in Structural Engineering*, vol. 19, no. 7, pp. 1165–1176, 2016.

[22] G. Sun, Q. Gu, and Y. Fang, "A simplified normalized cumulative hysteretic energy spectrum," *Earthquake and Structures*, vol. 12, no. 2, pp. 177–189, 2017.

[23] S. Dogru, B. Aksar, B. Akbas et al., "Parametric study on energy demands for steel special concentrically braced frames," *Steel and Composite Structures*, vol. 24, no. 2, pp. 265–276, 2017.

[24] M. Bruneau and N. Wang, "Some aspects of energy methods for the inelastic seismic response of ductile SDOF structures," *Engineering Structures*, vol. 18, no. 1, pp. 1–12, 1996.

[25] C. C. Chou and C. M. Uang, "An evaluation of seismic energy demand: an attenuation approach," Pacific Earthquake Engineering Research Center 2000/04, College of Engineering,University of California, Berkeley, Calif, USA, 2000.

[26] S. W. Geng, *Strong Ground Motion Input Parameter For Seismic Design [Doctor's Thesis]*, Institute of Engineering Mechanics ,China Earthquake Administration, Harbin, China, 2005.

[27] F. Guo, *Research on Some Issues of Site for Seismic Design [Master's Thesis]*, Huazhong University of Science and Technology, Wuhan, China, 2010.

[28] Y. Zhao, *Influence of site conditions on ground motion characteristics [Master's Thesis]*, Beijing University of Technology, Beijing, China, 2007.

[29] GB50011-2010, *Code for Seismic Design of Building*, Ministry of Housing and Urban-Rural Development of the People's Republic China, Beijing, China, 2010.

[30] H. S. Lv, *An earthquake Risk Analysis Method Based On Seismic Ground Motion Parameters [Doctor's Thesis]*, Institute of Geophysics,China Earthquake Administration, Beijing, China, 2005.

[31] GB18306-2015, *Seismic Ground Motion Parameter Zonation Map of China*, Standardization Administration of the People's Republic of China, Beijing, China, 2015.